Journal of Power Sources 380 (2018) 46–54

Contents lists available at ScienceDirect

Journal of Power Sources

journal homepage: www.elsevier.com/locate/jpowsour

Hydrogen oxidation mechanisms on Ni/yttria stabilized zirconia anodes: Separation of reaction pathways by geometry variation of pattern electrodes

M.C. Doppler[a,b], J. Fleig[b], M. Bram[a,c], A.K. Opitz[a,b,*]

[a] Christian Doppler Laboratory for Interfaces in Metal-Supported Electrochemical Energy Converters, Getreidemarkt 9/164-EC, 1060 Wien, Austria
[b] Institute of Chemical Technologies and Analytics, TU Wien, Getreidemarkt 9-164/EC, 1060 Vienna, Austria
[c] Institute of Energy Research (IEK-1) Forschungszentrum Jülich, Wilhelm-Johnen-Straße, D-52425 Jülich, Germany

HIGHLIGHTS

- Long term stable pattern anodes were prepared.
- Geometry variation allows separation of hydrogen oxidation pathways.
- Novel hydrogen oxidation pathway scaling with electrode area was identified.
- Area pathway explains current discrepancies existing in literature.

ARTICLE INFO

Keywords:
Microelectrode
Metal/solid electrolyte interface
SOFC anode
Electrochemical reaction kinetics
Impedance spectroscopy

ABSTRACT

Nickel/yttria stabilized zirconia (YSZ) electrodes are affecting the overall performance of solid oxide fuel cells (SOFCs) in general and strongly contribute to the cell resistance in case of novel metal supported SOFCs in particular. The electrochemical fuel conversion mechanisms in these electrodes are, however, still only partly understood. In this study, micro-structured Ni thin film electrodes on YSZ with 15 different geometries are utilized to investigate reaction pathways for the hydrogen electro-oxidation at Ni/YSZ anodes. From electrodes with constant area but varying triple phase boundary (TPB) length a contribution to the electro-catalytic activity is found that does not depend on the TPB length. This additional activity could clearly be attributed to a yet unknown reaction pathway scaling with the electrode area. It is shown that this area related pathway has significantly different electrochemical behavior compared to the TPB pathway regarding its thermal activation, sulfur poisoning behavior, and H_2/H_2O partial pressure dependence. Moreover, possible reaction mechanisms of this reaction pathway are discussed, identifying either a pathway based on hydrogen diffusion through Ni with water release at the TPB or a path with oxygen diffusion through Ni to be a very likely explanation for the experimental results.

1. Introduction

As global energy demand is expected to further increase in the future and emission of carbon dioxide is aimed to be reduced, novel and efficient energy conversion technologies are urgently required [1]. Solid oxide fuel cells (SOFCs) are compatible with a variety of possible future fuel infrastructures (e.g. hydrogen, or hydrocarbons synthesized from renewable resources) as they are capable of high chemical-to-electrical energy conversion efficiencies for a diverse set of fuels. State-of-the-art SOFCs utilize nickel/yttria stabilized zirconia (YSZ) cermet anodes on the fuel side, which usually perform well but under certain conditions may contribute significantly to the overall internal losses in the fuel cell, especially when operating with sulfur containing fuels. Moreover, in case of metal supported SOFCs the microstructure of the Ni/YSZ anode is usually less ideal than in electrolyte or anode supported systems. This is due to the fact that the anode sintering step during SOFC production is performed under reducing conditions facilitating Ni grain growth and thus increasing the anode polarization resistance [2,3].

Despite the importance of the anode for the efficiency of the overall SOFC system, the reaction mechanism of the most basic fuel reaction – the hydrogen oxidation – is still not very well understood [4–20]. On an

* Corresponding author. TU Wien, Institute of Chemical Technologies and Analytics, Christian Doppler Laboratory for Interfaces in Metal-Supported Electrochemical Energy Converters, Getreidemarkt 9/164-EC, 1060 Wien, Austria.
E-mail addresses: michael.doppler@tuwien.ac.at (M.C. Doppler), jfleig@mail.zserv.tuwien.ac.at (J. Fleig), m.bram@fz-juelich.de (M. Bram), alexander.opitz@tuwien.ac.at (A.K. Opitz).

https://doi.org/10.1016/j.jpowsour.2018.01.073
Received 12 October 2017; Received in revised form 22 January 2018; Accepted 24 January 2018
Available online 04 February 2018
0378-7753/

oxide ion conducting electrolyte the electrochemical hydrogen oxidation at the anode can be written in Kröger-Vink notation as follows:

$$H_2 + O_O^{\times} \rightleftarrows H_2O + V_O^{\cdot\cdot} + 2\,e' \quad (1)$$

In-depth understanding of mechanistic aspects, such as individual elementary steps of equation (1), are difficult to explore using commercial cermet anodes, particularly due to transport phenomena of ions, electrons and gaseous species within the porous network of a cermet anode contributing to the entire electrode polarization. This is why a number of previous studies dealing with hydrogen oxidation in Ni/YSZ electrodes utilized micro-patterned thin film Ni electrodes [4,6,12,15,20]. Besides usually avoiding problems arising from transport limitations, pattern electrodes also offer the opportunity of deliberate variation of the electrode geometry. Based on such geometry variations, these previous publications reported the rate limiting step of the hydrogen oxidation to be located at the triple phase boundary (TPB) between Ni, YSZ and the gas phase. In particular, this conclusion was obtained by measuring the polarization resistance of electrodes with varying TPB lengths and determining the exponent α of the following equation:

$$R_{Pol} = R_{Pol,0} \cdot l_{TPB}^{-\alpha} \quad (2)$$

In case the rate limiting step of the reaction is located at the triple phase boundary a value of 1 should be obtained for the exponent α. Measured values of α include 0.8 ± 0.04 [6], 0.67–1.2 [7], and 0.7–0.72 [20], thus significantly deviating from the expected α = 1. Moreover, also Refs. [4,21] noted deviations from proportionality between the inverse polarization resistance and the TPB length. As the aforementioned values of α are based on linear regression with very few data points, a more in-depth analysis of the published data is hardly possible. Consequently, a clear and unambiguous investigation of electrochemical pathways of H_2 oxidation on Ni/YSZ anodes is still lacking. For a knowledge-based optimization of anodes for metal supported SOFCs, as well as for a purposive increase of their sulfur tolerance, a more detailed understanding of the electrochemical hydrogen oxidation is needed.

In this contribution the deviations of the experimental data from the simple mechanistic picture of a solely TPB-active Ni anode are revisited by a detailed investigation of a large number of micro-patterned thin film Ni-electrodes employing different geometries at different temperatures and in different gas atmospheres containing H_2, H_2O and H_2S. In particular, numerous complex-shaped Ni thin film electrodes with different TPB lengths but nominally identical areas (and vice versa) were fabricated and electrochemically characterized at SOFC operation temperatures by impedance spectroscopy. On the basis of this data set, deviations from a simple geometrical relation between polarization resistance and TPB length could be clearly confirmed, which is supported by a detailed statistical analysis of the electrochemical results. Moreover, the deviation from a simple proportional relationship between TPB length and inverse polarization resistance is critically discussed in terms of an additional electrochemical H_2 oxidation pathway, which scales with the area of the Ni electrode and exists in parallel to the 'classical' TPB-path. The electrochemical properties of the two pathways are characterized in terms of their temperature dependence, sulfur poisoning behavior, as well as p_{H2} and p_{H2O} dependence. Based on these findings two possible reaction mechanisms are proposed for the area related pathway and possible connections with the TPB path are suggested. Discovery of the additional area-related H_2 oxidation pathway on Ni anodes thus further advances the understanding of the hydrogen oxidation at Ni/YSZ electro-catalysts and may serve as a basis for a knowledge-based optimization of SOFC cermet anodes.

2. Experimental

Micro-structured nickel thin film electrodes with a nominal film thickness of 1200 nm were prepared on (111)-oriented YSZ single crystals (Crystec, Germany) with pre-sintered NiO/YSZ counter electrodes by magnetron sputtering, photolithographic structuring, and chemical etching. The individual microelectrodes were then contacted by Ni tips and electrochemically characterized by impedance spectroscopy (Alpha A High Performance Frequency Analyzer, Novocontrol, Germany) in a homogeneously heated alumina reactor as depicted in Fig. 1. Four independent contacting tips were used to sequentially investigate four different microelectrodes in a single measurement run, for example at a constant temperature within a temperature sweep. This larger amount of measured microelectrodes significantly increases sample statistics. Impedance measurements were performed between 650 °C and 800 °C in different gas atmospheres, ranging from 2.5 kPa to 92 kPa H_2 and 0.15 kPa - 1.5 kPa H_2O. Further details on sample preparation and measurement procedure have already been published in previous work [19,22].

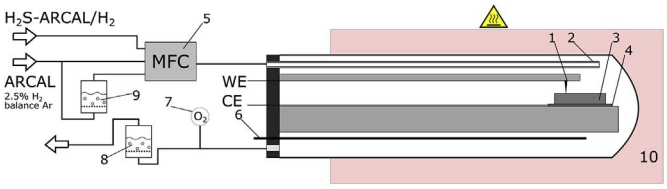

Fig. 1. Schematic drawing of the measurement setup. 1 Contacting needle (Ni), 2 Gas inlet, 3 sample, 4 counter electrode contact, 5 mass flow controller, 6 thermocouple, 7 lambda probe, 8 H_2S scrubber, 9 humidifier, 10 furnace.

All electrode geometries used are sketched in Fig. 2a while an optical micrograph and a scanning electron microscopy image of typical micro-patterned electrodes are shown in Fig. 2b and c, respectively. The exact sizes of all electrodes were determined by evaluation of microscopic images in a custom program; the results are discussed below. Altogether, 59 different electrodes with 15 different sizes or shapes were investigated.

The structural stability of electrodes under measurement conditions can be seen in comparing Fig. 2a and b. After over 700 h at standard measurement conditions no significant deviations in electrode structure like pore formation could be found.

3. Results

3.1. Analysis of the electrode geometries

In the electrode series with nominally constant area but varying circumference, area related effects are expected to be ideally constant

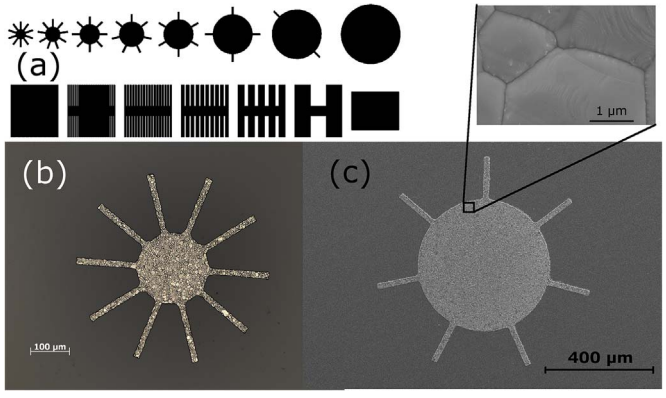

Fig. 2. (a) Depiction of the used electrode geometries on the lithographic mask. Up: Electrodes with nominally constant circumference/TPB length (decreasing circle size with compensation spikes). Down: Electrodes with nominally constant area (top and bottom areas are split into finger). (b) Reflected light microscopic image of a typical electrode after 720 h at 800 °C in H2.5W10 (2.5 kPa H_2, 0.15 kPa H_2O, balance Ar). (c) Electron microscopic image of a typical electrode with a higher magnification image at the top.

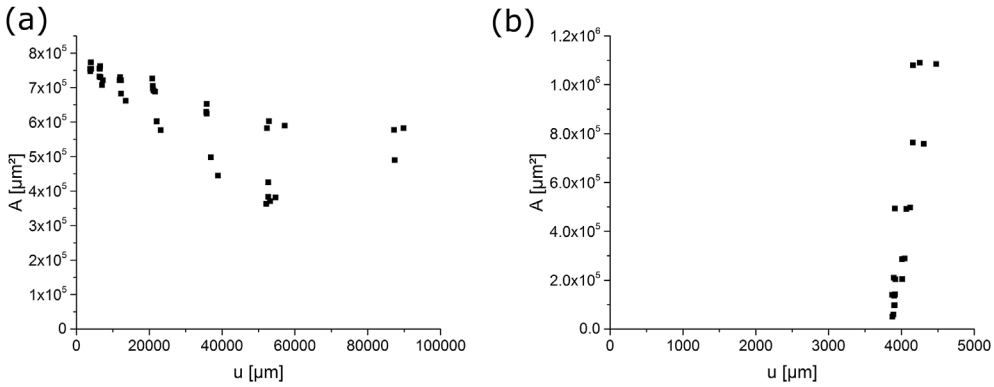

Fig. 3. (a) Microscopically measured area dependence on the circumference in nominally constant area electrodes. (b) Microscopically measured circumference dependence on the area for nominally constant circumference electrodes. The correlation between the properties is weak and scattering comparatively low.

on different microelectrodes. However, owing to slight over-etching during electrode preparation some minor deviations from this ideal picture may arise. Thus, the actual area and corresponding circumference of the investigated electrodes were measured and the results are shown in Fig. 3a. It can be seen that for a circumference increase of a factor of 23.8 the area at most decreases by a factor of only 2.1. Therefore the approximation of a constant area is sufficiently valid for this electrode series in cases where area effects are not dominant.

Analogously, in electrodes with nominally constant circumference but varying area electrochemical parameters originating from effects located at the triple phase boundary are expected to be constant. Actual measured areas and corresponding circumferences are shown in Fig. 3b. The plot shows that for an area increase by a factor of 21.3 the circumference increases by only a factor of 1.16. The assumption of constant circumference is therefore excellently met in this electrode series and more precise separation of area and TPB effects is therefore possible with this kind of electrodes. The average circumference of this type of electrodes, which is used to calculate TPB length specific conductances, is 4.03 mm.

3.2. Impedance spectra

The Nyquist plot of a typical impedance spectrum is plotted in Fig. 4a. The spectrum resembles a slightly asymmetric and depressed semicircle with an offset from the Z_{Re} axis. This spectrum was therefore fitted using a R_{Spread}-(R_{Pol}||CPE) equivalent circuit – which is shown as inset in Fig. 4a – where R_{Spread} is the spreading resistance of ion conduction in the electrolyte [23], R_{Pol} the polarization resistance of the electrode reaction (i.e., equation (1)) and CPE1 a constant phase element. This equivalent circuit is the same as used in our previous work where capacitances (deduced from the constant phase element) were discussed in detail [22]. However, due to the prime interest in the polarization resistance of the present paper, a slightly different fitting strategy was employed than in this previous work, to obtain more precise results for the polarization resistance: First, a spreading resistance value was determined by CNLS fitting the measured data to the equivalent circuit in Fig. 4a within the whole frequency range from 1 MHz to 5 mHz. Then the obtained spreading resistance was fixed and R_{Pol} as well as the CPE parameters were determined by another CNLS fit in the frequency range of 1 Hz–5 mHz. This procedure reduces the number of free fit parameters and thus helps coping with the slight asymmetry of the arc yielding a more accurate value for the "diameter" of the electrode feature. An example of the result of such a second fit is shown by the blue triangles/blue line in Fig. 4a.

3.3. Geometry dependencies

Electrodes with varying TPB length (and nominally constant area) as well as electrodes with varying area (and nominally constant circumference) were electrochemically characterized to determine the geometry dependence of the rate limiting step of hydrogen oxidation on micro-structured Ni/YSZ electrodes. In Fig. 4b the resulting polarization resistances of electrodes with varying TPB length measured at 800 °C in 2.5 kPa H_2 and 0.15 kPa H_2O (balance: Ar) are shown as a function of the circumference in a double-logarithmic plot. The slope of the linear fitting line in Fig. 4b, which is equivalent to the exponent α in equation (2), amounts to $\alpha = 0.66 \pm 0.056$. Hence, the inverse electrode polarization resistance is obviously not simply proportional the TPB length.

Conversely, Fig. 4c shows the conductance of electrodes with constant area from Fig. 4b as a function of their circumference in a linear plot. A linear fit of the pooled data from all measurement series reveals a line specific conductance of $(2.7 \pm 0.33)\cdot 10^{-5}\,Sm^{-1}$ and a bimodal distribution of the residuals. Moreover, a non-zero axis intercept was obtained from this linear fit, which is not in accordance with the expectation of purely TPB active Ni electrodes (cf. inset in Fig. 4c). Resulting parameters of all fits shown in Fig. 4c are summarized in Table 1. The different activity regimes may be the result of slightly different, individual conditions of the sample (e.g. different impurity levels at the surface of the crystals) as electrodes on one sample (characterized by the same measurement number in Fig. 4b and c) are mostly in the same regime. A more detailed investigation of this bimodal behavior, though scientifically interesting, is not the main goal of the present study and may be the topic of forthcoming work.

The main focus of the present paper deals with the analysis of the additional conductance contribution mentioned above. For the pooled fit and both activity regimes the $1/R_{Pol}$ intercept is found to be statistically significantly larger than 0 (see Table 1, $0 \notin CI95\%$). This means that besides the expected TPB length related conductance an additional conductance contribution is present on the investigated Ni thin film electrodes, which is independent of the TPB. Since the conductance is directly proportional to the equilibrium exchange rate of the H_2 oxidation reaction (equation (1)), the H_2 oxidation on the Ni/YSZ system can be concluded to proceed not only *via* the TPB. In other words, an additional electrochemical reaction pathway appears to be active, which is independent of the TPB length of the electrodes.

The conductance of constant-circumference electrodes plotted as a function of the area is depicted in Fig. 4d; the results of the shown linear fits are also summarized in Table 1. It can be seen that the conductance depends linearly on the area for each measurement series, with an obvious $1/R_{Pol}$-axis intercept. This $1/R_{Pol}$-axis intercept constitutes the expected behavior in case of purely TPB active electrodes (cf. inset in Fig. 4d) while the presence of the slope represents the activity of an additional reaction pathway. Since upon increasing the electrode area the contribution from the additional pathway increases this result clearly shows that besides the expected TPB-length related conductance an area-related conductance can be found. This area-related conductance suggests the existence of an additional area related reaction pathway; detailed discussion of this novel discovered path will be given in section 4.1.

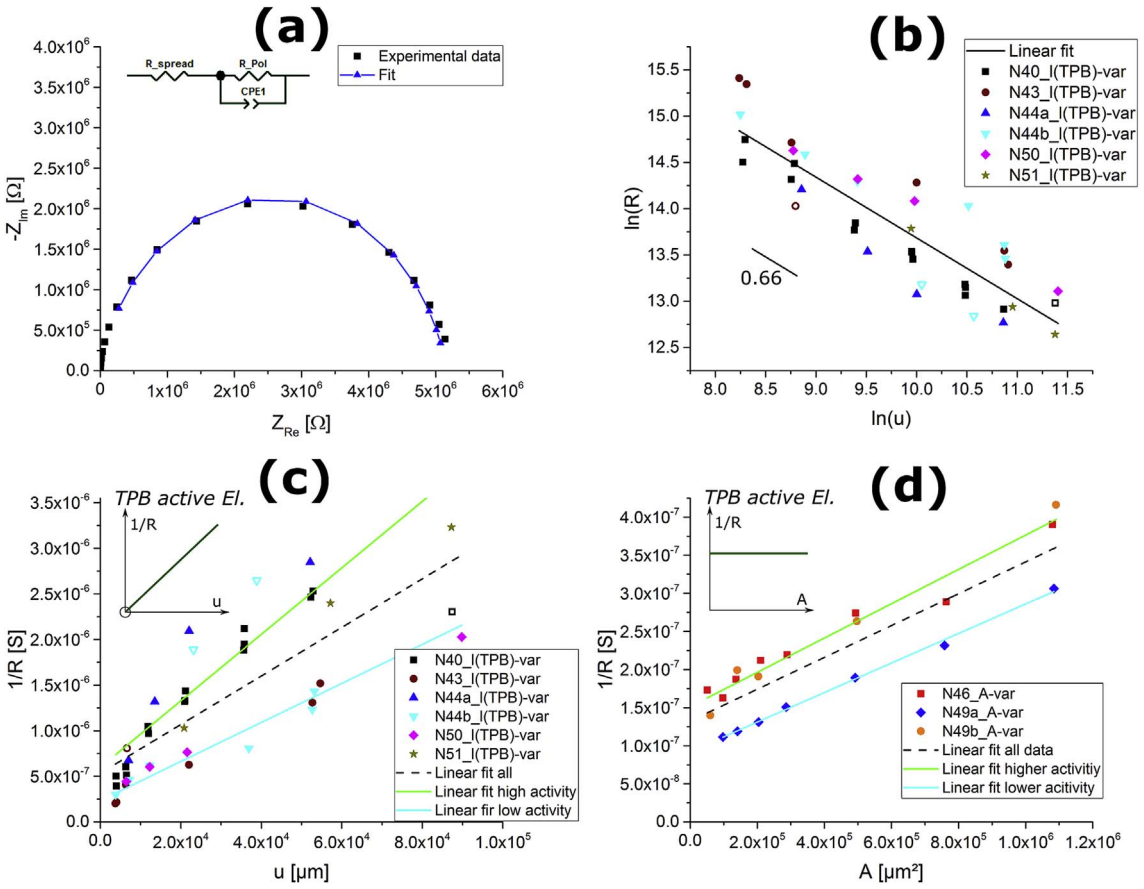

Fig. 4. (a) Typical impedance spectrum of a Ni/YSZ micro-patterned electrode. The fit was obtained by fixing the high frequency intercept and fitting in the frequency range of 1 Hz–5 mHz. Insert: Equivalent circuit used for fitting. (b) Electrode polarization resistance as a function of the circumference in a double-logarithmic plot. Open symbols indicate outliers and are not included in the linear fit. All closed symbols were included in a linear fit. (c) Electrode conductance (inverse polarization resistance) as a function of the circumference for nominally constant area electrodes (linear plot). The inset depicts the expected behavior of solely TPB-active electrodes with varying circumference. Fitting lines for all electrodes and high- and low-activity regimes are also plotted; open symbols denote outliers, which were not included in the linear fits. (c) Electrode conductance as a function of the area for electrodes with nominally constant circumference. The inset denotes the expected behavior of solely TPB-active electrodes. Fitting lines for all electrodes and high- and low-activity regimes are also plotted; open symbols denote outliers, which were not included in the linear fits. The sample number in the legends (with a,b) denotes the sequence number of the (partitioned) substrate crystal used for the sample, the letter N indicates a Ni layer. Conditions: 800 °C, H2.5W10 (2.5 kPa H_2, 0.15 kPa H_2O, balance Ar).

As series N46 and N49a seem to be shifted from series N49b, separate fitting was performed; the difference in slope between these fits, however, is not statistically significant on the 95% level (p = 0.13).

3.4. Hydrogen and water partial pressure

Electrodes with varying area (and nominally constant circumference) were electrochemically characterized in different atmospheres. Fig. 5 shows the area-dependence of the conductance for 3 different gas mixtures. In all cases a linear relationship between $1/R_{Pol}$ and electrode area was found. From the fitted slopes (denoted k) and $1/R_{Pol}$ intercepts (denoted d) for different gas mixtures, empirical reaction orders of the electrochemical hydrogen oxidation reaction can be obtained by plotting the conductances versus p_x in double-logarithmic diagrams and fitting to equation (3).

$$\ln(1/R) = \ln(1/R_0) + n \cdot \ln(p_x) \quad (3)$$

Therein 1/R denotes the (geometrically nominalized) conductance,

Table 1
Linear fit data of geometry dependencies in Fig. 4.

Data set		Slope	$1/R_{Pol}$ intercept
TPB length variation	All data	$(2.7 \pm 0.33)\cdot10^{-5}$ Sm^{-1}	$(5 \pm 1.2)\cdot10^{-7}$ S CI 95% [$2.9\cdot10^{-7}$,$7.8\cdot10^{-7}$] S
	High activity regime	$(3.6 \pm 0.31)\cdot10^{-5}$ Sm^{-1}	$(6 \pm 1.1)\cdot10^{-7}$ S CI 95% [$3.8\cdot10^{-7}$,$8.2\cdot10^{-7}$] S
	Low activity regime	$(2.3 \pm 0.43)\cdot10^{-5}$ Sm^{-1}	$(2.3 \pm 0.43)\cdot10^{-7}$ S CI 95% [$1.4\cdot10^{-7}$,$3.3\cdot10^{-7}$] S
Area variation	All data	0.21 ± 0.025 S/m^{-2}	$(1.3 \pm 0.13)\cdot10^{-7}$ S Normalized: $(3.2 \pm 0.32)\cdot10^{-5}$ Sm^{-1}
	High activity regime	0.23 ± 0.013 S/m^{-2}	$(1.51 \pm 0.069)\cdot10^{-7}$ S Normalized: $(3.7 \pm 0.17)\cdot10^{-5}$ Sm^{-1}
	Low activity regime	0.194 ± 0.0046 S/m^{-2}	$(9.2 \pm 0.26)\cdot10^{-8}$ S Normalized: $(2.28 \pm 0.065)\cdot10^{-5}$ Sm^{-1}

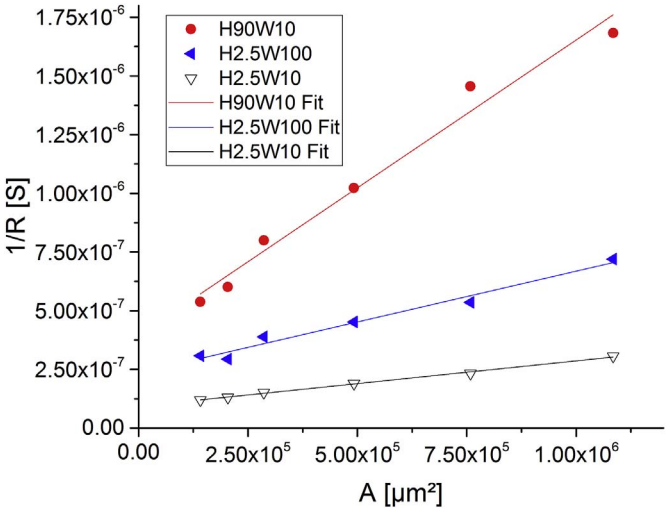

Fig. 5. Electrode conductance as a function of the area of electrodes with nominally constant circumference for 3 gas mixtures. Conditions: 800 °C; H90W10 = 92.5 kPa H_2, 0.15 kPa H_2O; H2.5W10 = 2.5 kPa H_2, 0.15 kPa H_2O, H2.5W100 = 2.5 kPa H_2, 1.5 kPa H_2O.

p_x the partial pressure of the gas x and n the empirical reaction order. For hydrogen, the empirical reaction order for the area pathway (represented by the slope) was 0.51 ± 0.053 (Fig. 6a), while the empirical reaction order for the TPB pathway (represented by the $1/R_{Pol}$ intercept) was 0.39 ± 0.043 (Fig. 6d). For water, the empirical reaction orders for the area pathway were 0.35 ± 0.11 and 0.35 ± 0.11 for the TPB pathway (Fig. 6d) and area pathway (Fig. 6b), respectively.

Moreover, an equivalent oxygen partial pressure was calculated from the H_2: H_2O ratios using NIST data [24] and all data points plotted in double-logarithmic diagrams in the same way as above yielding Fig. 6c and f. It can be seen that there is no simple linear trend neither in the log(p_{O2})-log(k) nor in the log(p_{O2})-log(d) diagram.

3.5. Sulfur poisoning

Fig. 7a shows the inverse electrode polarization resistance of electrodes with varying area (i.e., nominally constant circumference) as a function of the electrode area before and after 10 ppm H_2S were added to the gas feed. The slope decreases from 0.20 ± 0.016 Sm^{-2} in the pristine state to 0.162 ± 0.0094 Sm^{-2} in the sulfur poisoned state – corresponding to an activity decrease by ca. 20%. The $1/R_{Pol}$ intercept decreases from (1.58 ± 0.081)·10^{-7} S to (8.2 ± 0.49)·10^{-8} S, which is an decrease in activity by almost a factor of 2. This strongly different behavior of TPB and area pathway upon H_2S poisoning clearly points

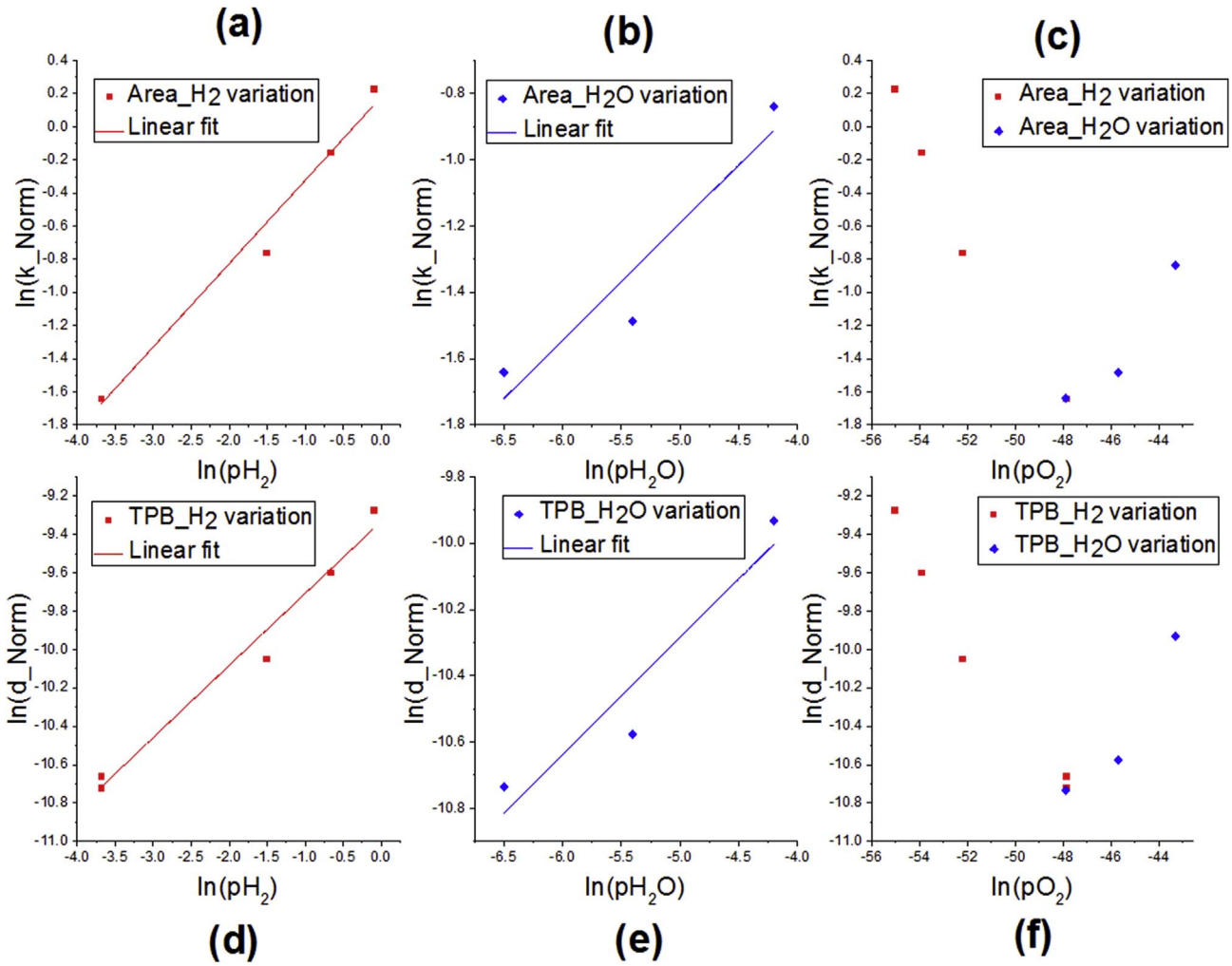

Fig. 6. Determination of empirical reaction orders for H_2 and H_2O. The diagrams show the slopes and $1/R_{Pol}$ intercepts of measurements in different gas atmospheres (see Fig. 7) as a function of the respective partial pressure in double-logarithmic plots. a–c: Slopes (correspond to area pathway) as a function of hydrogen, water and equilibrium oxygen partial pressure, respectively. d–f: $1/R_{Pol}$ intercepts (correspond to TPB pathway) normalized to the circumference as a function of hydrogen, water and equilibrium oxygen partial pressure, respectively. a,d: Constant p_{H2O} of 0.15 kPa. b,e: Constant p_{H2} of 2.5 kPa. For all: 800 °C, balance gas Ar.

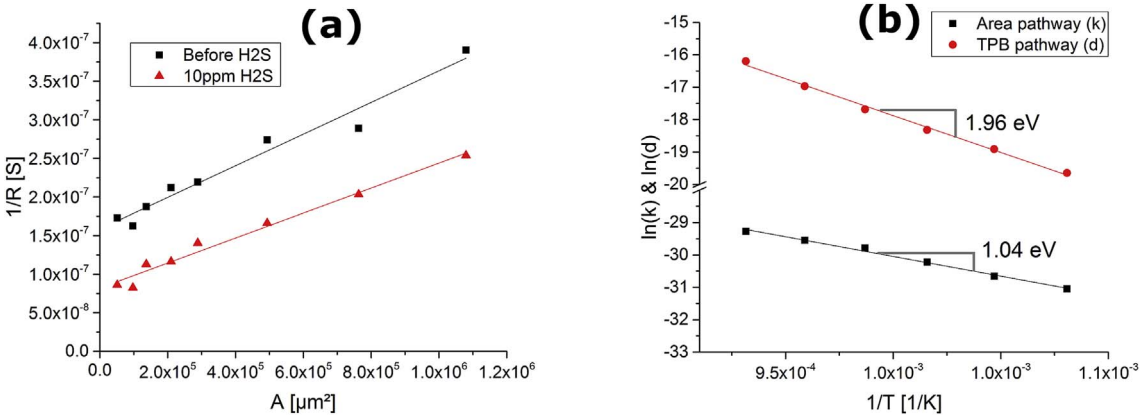

Fig. 7. (a) Investigation of the effect of 10 ppm H_2S addition on the conductance of nominally constant circumference electrodes as a function of the electrode area. Conditions: 800 °C, 2.5 kPa H_2, 0.15 kPa H_2O, (0.001 kPa H_2S), balance Ar. (b) Arrhenius plot for the slope (k in the diagram) and $1/R_{Pol}$ intercept (d in the diagram). Slopes and $1/R_{Pol}$ intercepts were obtained by measuring nominally constant circumference electrodes at varying temperatures and fitting analogously to Fig. 6b. Conditions: H2.5W10.

out their different nature.

3.6. Activation energy

The electrochemical polarization resistance of electrodes with varying area was characterized also at varying temperatures. Fig. 7b shows the corresponding Arrhenius plot for slope and $1/R_{Pol}$ intercept, which were obtained by the same procedure as discussed above (see section 3.3). For the area pathway an activation energy of 1.04 ± 0.044 eV is obtained from Fig. 7b, while the activation energy for the TPB pathway is determined as 1.96 ± 0.069 eV. This strong difference in activation energy is thus another strong indication for a completely different rate limiting step of the two pathways for the same net reaction (which is the H_2 oxidation reaction in equation (1)).

4. Discussion

4.1. Geometric correlation to reaction pathways

As mentioned above in section 1, 'sublinear scaling' of the inverse polarization resistance with the TPB length ($\alpha < 1$ in equation (2)) has already been reported in literature [6,7,20]. but has not been discussed in detail so far. This deviant behavior from the ideal linear scaling is reproduced in this study, as shown in section 3.3, with an exponent α of 0.66. Yao and coworkers explained this deviancy by assuming an unaccounted series resistance [20].

Another explanation for this sublinear scaling can be given by a parallel, non-TPB length dependent resistance. This hypothesis entails that in a non-logarithmic plot of the conductance $1/R_{Pol}$ *versus* the triple phase boundary length a linear relationship is expected to be found with a positive conductance intercept, since conductances of parallel resistors add up. Exactly such a linear relationship with $1/R_{Pol}$ -axis intercept can be found in Fig. 6a, and as shown in Table 1 the conductance intercepts are statistically significantly bigger than 0. It can therefore be concluded that this parallel resistor hypothesis is plausible.

The most likely source for the additional conductance is an additional reaction pathway with a rate limiting step not located at the triple phase boundary. Since the area is nominally kept constant in electrodes measured in Fig. 6a a reaction pathway with a rate limiting step scaling with the area is a reasonable hypothesis. This hypothesis predicts a linear relationship between the area and the conductance of electrodes with constant triple phase boundary length. The conductance intercept in this case corresponds to the triple phase boundary activity. Fig. 6b shows that this linear relationship with a slope > 0 indeed exists and the normalized intercepts of high and low activity regime (see Table 1) amount to $(3.8 \pm 0.17)\cdot10^{-5}\,Sm^{-1}$ and $(2.29 \pm 0.063)\cdot10^{-5}\,Sm^{-1}$, which is in excellent agreement with the values obtained on the constant area electrodes of $(3.6 \pm 0.31)\cdot10^{-5}\,Sm^{-1}$ and $(2.3 \pm 0.43)\cdot10^{-5}\,Sm^{-1}$, respectively. This dependency of the conductance on the area and its consistency with the behavior of electrodes of constant area strongly supports our interpretation in terms of an additional area-scaling reaction pathway for the hydrogen oxidation on Ni/YSZ electrodes.

4.2. Properties of area- and TPB length scaling pathways

4.2.1. H_2 and H_2O partial pressure dependency

As shown in section 3.4 the empirical reaction orders of water for both the TPB length and area-scaling pathway are not distinguishable. This means that previous work, irrespective of the contribution from a possible area pathway, should be in agreement with the empirical reaction order found here. While results of Yao and Croiset (0.3 at 700 °C) [20] as well as de Boer (0.35 at 850 °C) [21] are in good agreement with this work, Utz and coworker (0.68 at 800 °C) [15] as well as Bieberle and coworker (0.67 at 700 °C) [7] found different values. Mizusaki and coworker [4] found non-linearities in the $\log(1/R_{Pol})$ vs. $\log(p_{H2O})$ plots at lower temperatures (700 °C), which disappeared at temperatures of 800 °C and higher; they report an empirical reaction order of 0.86 at 850 °C.

In terms of the empirical reaction order of H_2 a slight difference was found between the area scaling pathway (0.51 ± 0.053) and the TPB length scaling pathway (0.39 ± 0.043). Previous studies report smaller values for the empirical hydrogen reaction order, ranging from −0.26 to 0.145 [4,7,15,20,21]. This substantial scattering between different studies, including the result in this work, seems to indicate that some processes in the reaction cascade are influenced by yet unknown factors.

4.2.2. Sulfur poisoning

In the sulfur poisoning experiments it was found that the TPB length scaling pathway is significantly affected by the addition of 10 ppm H_2S, indicated by an increase in the TPB length specific resistance by a factor of ca. 2 (see section 3.5). The effect on the area scaling pathway, on the other hand, is much smaller with an increase in the area specific resistance of only about 20%. This result not only supports the 2 reaction pathway model of hydrogen oxidation on Ni/YSZ electrodes, but also shows that besides the 'classical' TPB length scaling pathway, which is indeed strongly affected by sulfur poisoning, an additional more sulfur resilient reaction pathway exists in the Ni/YSZ system. This characteristic of the area related path may offer the possibility of obtaining more sulfur resistant Ni/YSZ anodes for SOFCs, by tuning cermet anodes towards more area-pathway dominated kinetics.

4.2.3. Activation energy

The geometry dependent investigation of the thermal activation revealed 1.96 eV and 1.04 eV for the TPB length and area scaling pathways, respectively. Given that in previous studies a convolution of both pathway contributions was measured, two activation energies may be found for a given electrode geometry with the lower activation energy dominating at lower temperatures. Such a result was indeed obtained qualitatively by Yao and Croiset, although the absolute values for the activation energy are not in accordance with this study [20].

4.3. Reaction mechanisms

4.3.1. Electrochemical reaction pathways

In this section, the above described findings will be discussed in terms of parallel reaction pathways for the electrochemical hydrogen oxidation on our micro-patterned Ni electrodes and their possible connections. In the analysis of the geometry dependence of the electrode polarization resistance two parallel resistive contributions were identified – one originating from a rate limiting step located close to the TPB and the other one being associated to a rate limiting process scaling with the electrode area. This situation is sketched by the equivalent circuit in Fig. 8a. In such an equivalent circuit a parallel faradaic pathway represents an additional possibility for the electrode reaction to proceed. A resistance in the equivalent circuit shows that for a current flow *via* the faradaic path an overpotential needs to be applied to drive the reaction. This overpotential is mainly 'consumed' in the rate limiting step(s) of the reaction. If the inverse polarization resistance, i.e. the conductance, is proportional to the electrode area or to its TPB length/circumference, this indicates that the rate limiting reaction site is associated to the respective geometric property. Fast reaction steps that might occur before or after the rate limiting step are, however, not necessarily restricted to the same location. The terms TPB length and area related pathways therefore only imply that the rate limiting step is restricted to a sufficiently small region at the TPB or to a site proportional to the area of the electrode, respectively. The corresponding site of the area pathway can be either related to the Ni/YSZ interface, the electrode bulk (including grain boundaries) or the Ni surface. Possible mechanisms explaining the equivalent circuit in Fig. 8a thus need to exhibit rate limiting steps with the corresponding geometry dependence.

Another experimental observation, which needs to be considered by a reaction mechanism, is the virtually identical behavior of TPB and area pathway on water partial pressure variation, (see section 3.4). While the polarization resistance gives rather direct information on the kinetics of the rate limiting step, the dependency on gas partial pressures may also be affected by elementary steps prior or subsequently to the rate limiting one. Reaction steps not causing significant polarization resistances are very close to the equilibrium state. These equilibria can be influenced by the partial pressure of involved gas species, which as a consequence can change the concentration of the reactants in the rate limiting step and thus may also affect the overall reaction rate. The dependency on partial pressures can therefore not only provide information on the rate limiting step, but it can also yield insights into non-rate limiting steps. This means that the almost identical water partial pressure dependence of both pathways, even though it may contain some statistical uncertainty, provides at least an indication for a convergence of both reaction pathways on the water-side of the reaction chain.

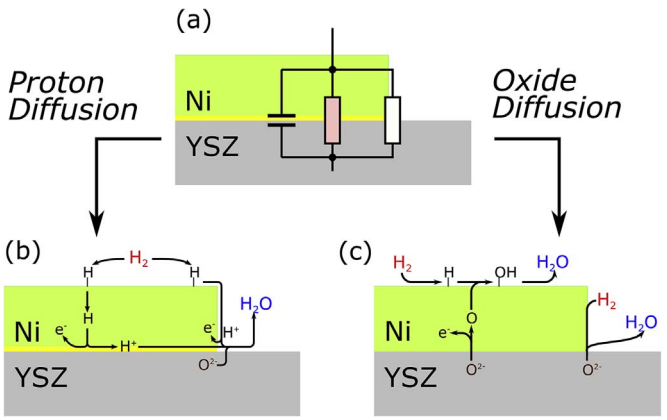

Fig. 8. Possible schematic reaction mechanisms for the hydrogen oxidation in Ni/YSZ. (a) Sketch of the discussed equivalent circuit indicating different locations of the two identified faradaic reaction pathways. (b) Proton diffusion mechanism (c) Oxide diffusion mechanism.

Considering these thoughts, two possible reaction mechanisms for the area pathway are suggested, which are schematically illustrated in Fig. 8b and c. Especially the mechanisms of the area pathway, their potential rate limiting steps, and their connection with a TPB-related reaction pathway will be discussed in detail in the following.

4.3.2. Proton diffusion path

The first mechanism for the area pathway – sketched in Fig. 8b – describes the dissociative adsorption of hydrogen on the Ni surface, diffusion of H through the Ni film, and charge transfer at the Ni/YSZ interface. The formed protons diffuse along the Ni/YSZ interface to the TPB, and finally recombine with oxide ions from the electrolyte to form water, which desorbs. The assumption of such a proton transport step along an electrode/electrolyte interface, which may sound peculiar on a first glance, is necessary because water would be trapped at the interface and could not escape to the gas phase. Moreover, high resolution electron microscopy images on cross sections of our Ni thin film electrodes reveal a ca. 1 nm thin oxidic layer at the interface (cf. fig. 9 in Ref. [21]), which may provide the required proton conductivity. Owing to the observed area dependence, proton transport along this phase needs to be fast, even at the macroscopic scale of the electrode size (the maximum diameter here is 1200 µm, thus maximum diffusion length for protons along the interface would be around 600 µm), which is not unrealistic at these elevated temperatures. The convergence with the TPB pathway, which is required to explain the observed p_{H2O} dependence, occurs at the TPB where protons from the interface and protons produced from charge transfer at the TPB meet, both forming water with oxide ions from YSZ. The recombination and water desorption step is thus identical for both pathways.

As rate limiting step of the area pathway, hydrogen adsorption/dissociation on the surface, hydrogen diffusion through the bulk or a charge transfer step at the Ni/YSZ interface could explain the observed geometry dependence since all scale with the electrode area. The polarization resistance in case of bulk diffusion limitation can be obtained by

$$R_{diff} = \frac{kT}{z^2e^2}\frac{L_D}{Dn_{eq}} \quad (4)$$

with R_{diff} the polarization resistance, k the Boltzmann constant, T the absolute temperature, z the number of transferred elementary charges, e the elementary charge, L_D the diffusion length, D the diffusion coefficient and n_{eq} the equilibrium concentration of the diffusing species [25]. With the diffusion coefficient and bulk concentration of hydrogen in nickel at 800 °C from Ref. [26] and an electrode thickness of 1.2 µm this results in a conductance $1/R_{diff} = 2.8*10^3\,Sm^{-2}$, which is 4 orders of magnitude higher than the measured value of 0.19 S/m^2. Hydrogen diffusion through Ni is therefore way too fast to act as the rate limiting step. Since dissociative adsorption of hydrogen on Ni is fast [27], a charge transfer step at the interface appears to be the most likely rate limiting step in this mechanism.

4.3.3. Oxide diffusion path

The second mechanism reverses the role of the species. Instead of

hydrogen diffusing towards the Ni/YSZ interface, oxygen moves towards the free Ni surface – see the sketch in Fig. 8c. That means that oxide ions from the electrolyte are electrochemically oxidized at the Ni/YSZ interface, the formed O diffuses through the Ni electrode and recombines with H on the surface of Ni to form water. As rate limiting steps for this area pathway charge transfer of oxide ions at the Ni/interface, oxygen diffusion through the Ni bulk, a reaction at the surface or desorption of water may be considered. Using equation (4) as well as the diffusion coefficient and equilibrium concentration of oxygen in Nickel from Ref. [28], an oxygen diffusion limited conductance of $1/R_{diff} = 2.6\,Sm^{-2}$ can be calculated. This value, while still being an order of magnitude too high, could explain the experimental data, since results in Ref. [28] do not exactly correspond to measurement conditions as they were obtained on Ni in equilibrium with NiO – i.e., under more oxidizing conditions. Thus, the concentration of diffusing oxygen may be significantly lower for the Ni thin films here than in case of the study in Ref. [28], making oxygen diffusion a likely candidate for the rate limiting step in this model. A similar oxygen diffusion pathway through a predominantly TPB active electrode was also already found for the system $Pt(O_2)$/YSZ [29–31]. There, oxygen diffusion along Pt grain boundaries was identified as the rate limiting elementary step for the area dependent pathway. Since the Ni thin films here do also contain sufficient amounts of grain boundaries (cf. Fig. 2) also in this case an oxygen transport path along Ni grain boundaries may be a feasible explanation for the area related pathway.

A possible variant of the oxygen diffusion pathway could be a hydroxyl diffusion mechanism, which may occur in case of recombination of O and H already within the Ni bulk. Since hydrogen diffusion in Ni was shown above to be very fast under the present conditions, such a hydroxyl diffusion mechanism may only be hardly distinguishable from a “pure” oxygen diffusion through Ni since diffusion coefficients of O and OH may be similar due to their similar size.

Convergence of pathways, as suggested by the identical water partial pressure dependence, could happen at the water desorption step, provided it occurs on the Ni surface. For the TPB related pathway this kind of mechanism, where oxide ions diffuse from the oxide surface onto the Ni surface, has been discussed in literature as ‘oxygen spillover’ [12].

4.3.4. Electronic conductivity in YSZ as a potential artifact mimicking a parallel electrode pathway

While YSZ is widely known to be an electronically blocking and ionically conducting material, a certain residual electronic conductivity, especially in reducing atmospheres, can be found, see e.g. Ref. [32]. This electronic conductivity provides a parallel electronic pathway from the working to the counter electrode that could feign a parallel electrochemical reaction pathway. Since the electrons in the electrolyte spread the same way ions do, the expected electronic parallel resistance can be calculated via the relation

$$\frac{\sigma_{eon}}{\sigma_{ion}} = \frac{R_{ion}}{R_{eon}} \tag{5}$$

with σ the ionic and electronic conductivity and R the ionic and electronic spreading resistance, respectively. For 800 °C and a p_{H2}:p_{H2O} ratio of 2.5/0.15 the conductivities are $\sigma_e = 1.24{\cdot}10^{-6}\,Scm^{-1}$ [32], and $\sigma_i = 0.0392\,Scm^{-1}$, [33]. At this temperature an ionic spreading resistance of $R_{ion} = 125\,\Omega$ was measured on the largest electrode with nominally constant circumference (high frequency intercept of the impedance spectrum, see section 3.2). From these values an electronic spreading resistance of 3.9 MΩ follows from equation (5). This spreading resistance is in remarkable agreement with the observed polarization resistance of the area pathway of ~4.4 MΩ (TPB pathway share not included). There are, however, several objections to the hypothesis that the area scaling pathway originates from electronic conductivity in the YSZ:

- The electronic conductivity in YSZ shows an activation energy of 3.88 eV [32] which does not explain the observed activation energy of 1.04 eV for the area pathway in the present experiments. Hence, at 650 °C the measured polarization resistance of 24 MΩ does not fit the calculated value of 650 MΩ.
- Moreover, the electronic conductivity in YSZ is predicted to be proportional to $p_{O2}^{-1/4}$. While this relationship has been found in the hydrogen partial pressure variation, (hydrogen reaction order of 0.51 is equivalent to $p_{O2}^{-0.26}$), the dependence on the water partial pressure clearly defies this prediction.
- Finally, a different geometry dependence is expected, because for circular electrodes the inverse spreading resistance is proportional to the diameter of the electrode [23,34]. Since the shape of the investigated electrodes is relatively close to circles, a non-linearity between area and inverse polarization resistance would result in case of electronic conductivity in YSZ playing a role, which was not found experimentally.

Since the electronic path in the YSZ electrolyte is predicted by conductivity values in Ref. [32] but not observed in the data in this study, the electrons may be most likely blocked at the Ni/YSZ interface. This could be due to a Schottky-contact between the materials creating a highly resistive Ni/YSZ-interface while still allowing for electronic YSZ conductivity or due to a foreign phase at the interface which blocks electrons but is sufficiently permeable for oxide ions. The interfacial oxide found by TEM in a previous study on our Ni/YSZ electrodes – see Fig. 9 in Ref. [21] – may provide such an electronically blocking layer between electrode and electrolyte.

5. Conclusions

In this study, micro-structured Ni thin film electrodes on YSZ were employed to investigate reaction pathways for hydrogen oxidation. In order to achieve statistically sound conclusions a significantly larger sample size was measured than usually used in literature. Measurements on electrodes with varying TPB length but nominally constant area revealed a TPB length specific inverse polarization resistance of $2.7{\cdot}10^{-5}\,Sm^{-1}$ at 800 °C (2.5 kPa H_2, 0.15 kPa H_2O, balance Ar). Owing to its geometry dependence this conductance can be concluded to originate from an electrochemical reaction pathway with a rate limiting step located close the TPB. Besides, the electrode's TPB activity showed a bimodal distribution with TPB length specific conductances of $3.6{\cdot}10^{-5}\,Sm^{-1}$ and $2.3{\cdot}10^{-5}\,Sm^{-1}$ for the high and low activity regime, respectively.

In addition to the TPB length process an additional conductance, statistically significantly larger than 0, was found. By measurements on electrodes with constant TPB length but varying area, the additional contribution to the electrode activity could be attributed to a process proportional to the electrode area with an area specific conductance of $0.194\,Sm^{-2}$. This additional area related conductance can therefore be interpreted as a parallel reaction pathway, with a rate limiting step located either on the Ni surface, in the Ni bulk or at the Ni/YSZ interface.

It could be clearly shown that this newly discovered reaction pathway shows different electrochemical behavior than the TPB pathway. The activation energy of the area scaling pathway was found to be 1.04 eV, while the TPB length scaling pathway was activated with 1.96 eV. The effect of adding 10 ppm H_2S to the atmosphere was more severe for the TPB scaling pathway (polarization resistance increase by about a factor of 2) than for the area scaling one (polarization resistance increase by ca. 20%). Also, while no difference in the empirical reaction order for water was found (0.35 for both pathways), a small difference for the hydrogen reaction order was found (0.51 for the area pathway, 0.39 for the TPB pathway).

Two reaction mechanisms appear to be the most plausible explanations for the observed area scaling pathways: One feasible

reaction pathway is adsorption of hydrogen on the Ni surface and H diffusion through the electrode to the Ni/YSZ interface where charge transfer takes place. The protons then diffuse to the TPB along the electrode interface where they recombine with oxide ions to form water. For this lateral proton diffusion a foreign phase at the interface may play an important role. Another very likely possibility is that oxide ions from the YSZ electrolyte get oxidized at the Ni/YSZ interface diffusing as O through Ni to the electrode surface where they react with adsorbed hydrogen to form water.

Since this newly discovered area scaling pathway shows more sulfur resilience compared to the TPB scaling pathway, research in origins of and influences on the pathway may lead to more sulfur resilient SOFC anodes, e.g. by respective optimization of the microstructure of Ni/YSZ cermet anodes, doping of the Ni metal or by modifications of the Ni/electrolyte interface, which may enhance the electrochemical performance of this additional pathway.

Acknowledgement

The financial support by the Austrian Federal Ministry of Science, Research and Economy and the National Foundation for Research, Technology and Development is gratefully acknowledged.

Huber Scientific (sofc.at) is acknowledged for supporting the development of the micro contact test station used in this study.

Glossary

SOFC	Solid oxide fuel cell
YSZ	Yttrium stabilized zirconia
TPB	Triple phase boundary

References

[1] S. Chu, A. Majumdar, Opportunities and challenges for a sustainable energy future, Nature 488 (7411) (2012) 294–303.
[2] M. Haydn, et al., Development of metal supported solid oxide fuel cells based on powder metallurgical manufacturing route, Powder Metall. 56 (5) (2013) 382–387.
[3] V.A. Rojek-Wöckner, et al., A novel Ni/ceria-based anode for metal-supported solid oxide fuel cells, J. Power Sources 328 (Supplement C) (2016) 65–74.
[4] J. Mizusaki, et al., Preparation of nickel pattern electrodes on YSZ and their electrochemical properties in H 2 - H 2 O atmospheres, J. Electrochem. Soc. 141 (8) (1994) 2129–2134.
[5] J. Mizusaki, et al., Kinetic studies of the reaction at the nickel pattern electrode on YSZ in H2-H2O atmospheres, Solid State Ionics 70–71 (1994) 52–58 Part 1(0).
[6] A. Bieberle, L.J. Gauckler, Reaction mechanism of Ni pattern anodes for solid oxide fuel cells, Solid State Ionics 135 (1–4) (2000) 337–345.
[7] A. Bieberle, L.P. Meier, L.J. Gauckler, The electrochemistry of Ni pattern anodes used as solid oxide fuel cell model electrodes, J. Electrochem. Soc. 148 (6) (2001) A646–A656.
[8] D. Kek, M. Mogensen, S. Pejovnik, A study of metal (Ni, Pt, Au)/Yttria-Stabilized zirconia interface in hydrogen atmosphere at elevated temperature, J. Electrochem. Soc. 148 (8) (2001) A878–A886.
[9] K.V. Jensen, et al., Effect of impurities on structural and electrochemical properties of the Ni–YSZ interface, Solid State Ionics 160 (1–2) (2003) 27–37.
[10] A.M. Sukeshini, et al., Electrochemical oxidation of H2, CO, and CO / H2 mixtures on patterned Ni anodes on YSZ electrolytes, J. Electrochem. Soc. 153 (4) (2006) A705–A715.
[11] M. Vogler, et al., Modelling study of surface reactions, diffusion, and spillover at a Ni/YSZ patterned anode, J. Electrochem. Soc. 156 (5) (2009) B663–B672.
[12] W.G. Bessler, et al., Model anodes and anode models for understanding the mechanism of hydrogen oxidation in solid oxide fuel cells, Phys. Chem. Chem. Phys. 12 (42) (2010) 13888–13903.
[13] A. Ehn, et al., Electrochemical investigation of nickel pattern electrodes in H2/H2O and CO/CO2 atmospheres, J. Electrochem. Soc. 157 (11) (2010) B1588–B1596.
[14] M.V. Rao, et al., The influence of the solid electrolyte on the impedance of hydrogen oxidation at patterned Ni electrodes, Solid State Ionics 181 (25–26) (2010) 1170–1177.
[15] A. Utz, et al., Degradation and relaxation effects of Ni patterned anodes in H2 – H2O atmosphere, J. Electrochem. Soc. 157 (6) (2010) B920–B930.
[16] A. Utz, et al., Impurity features in Ni-YSZ-H2-H2O electrodes, Solid State Ionics 183 (1) (2011) 60–70.
[17] W. Yao, E. Croiset, Ni/YSZ pattern anodes fabrication and their microstructure and electrochemical behavior changes in H2–H2O environments, J. Power Sources 226 (0) (2013) 162–172.
[18] W. Yao, E. Croiset, Modelling and Ni/Yttria-Stabilized-Zirconia pattern anode experimental validation of a new charge transfer reactions mechanism for hydrogen electrochemical oxidation on solid oxide fuel cell anodes, J. Power Sources 248 (0) (2014) 777–788.
[19] M.C. Doppler, J. Fleig, A.K. Opitz, The influence of sulfur poisoning and YSZ substrate orientation on electrochemical properties of nickel pattern anodes, ECS Trans. 68 (1) (2015) 1383–1390.
[20] W. Yao, E. Croiset, Stability and electrochemical performance of Ni/YSZ pattern anodes in H2/H2O atmosphere, Can. J. Chem. Eng. 93 (12) (2015) 2157–2167.
[21] B. de Boer, SOFC Anodes : Hydrogen Oxidation at Porous Nickel and Nickel/yttria-stabilised Zirconia Cermet Electrodes, Universiteit Twente, Netherlands, 1998.
[22] M.C. Doppler, et al., The capacitance of nickel pattern electrodes on zirconia electrolyte, J. Electrochem. Soc. 163 (10) (2016) H1019–H1025.
[23] F.S. Baumann, et al., Impedance spectroscopic study on well-defined (La,Sr)(Co,Fe) O3 − δ model electrodes, Solid State Ionics 177 (11–12) (2006) 1071–1081.
[24] P.J. Linstrom, W.G. Mallard (Eds.), NIST Chemistry WebBook, NIST Standard Reference Database Number 69, National Institute of Standards and Technology, 2005.
[25] Carl H. Hamann, W.V., Elektrochemie, fourth ed., WILEY-VCH, Germany, 2005.
[26] S.-M. Lee, J.-Y. Lee, The trapping and transport phenomena of hydrogen in nickel, Metall. Trans. 17 (2) (1986) 181–187.
[27] A. Hamza, R. Madix, Dynamics of the dissociative adsorption of hydrogen on nickel (100), J. Phys. Chem. 89 (25) (1985) 5381–5386.
[28] J.-W. Park, C.J. Altstetter, The diffusion and solubility of oxygen in solid nickel, Metall. Trans. 18 (1) (1987) 43–50.
[29] A.K. Opitz, et al., Investigation of the oxygen exchange mechanism on Pt|yttria stabilized zirconia at intermediate temperatures: surface path versus bulk path, Electrochim. Acta 56 (27) (2011) 9727–9740.
[30] T. Ryll, et al., Microscopic and nanoscopic three-phase-boundaries of platinum thin-film electrodes on YSZ electrolyte, Adv. Funct. Mater. 21 (3) (2011) 565–572.
[31] T.M. Huber, A.K. Opitz, J. Fleig, Oxygen reduction via grain boundary transport in thin film platinum electrodes on yttria stabilized zirconia, Solid State Ionics 273 (2015) 8–12.
[32] J.H. Park, R.N. Blumenthal, Electronic transport in 8 mole percent Y 2 O 3 - ZrO2, J. Electrochem. Soc. 136 (10) (1989) 2867–2876.
[33] A.K. Opitz, J. Fleig, Investigation of O2 reduction on Pt/YSZ by means of thin film microelectrodes: the geometry dependence of the electrode impedance, Solid State Ionics 181 (15–16) (2010) 684–693.
[34] J. Newman, Resistance for flow of current to a disk, J. Electrochem. Soc. 113 (5) (1966) 501–502.